THE ROYAL SOCIETY

A reusable space-rescue vehicle: re-entry simulation

By R. A. East

Department of Aeronautics and Astronautics, University of Southampton, Southampton SO17 1BJ, UK

This paper presents the conceptual design of a re-entry vehicle suitable for the emergency return of personnel from the International Space Station. For injured occupants, or those with emergency medical conditions, a re-entry environment with a maximum g loading of less than 1.1 would be necessary. This has been met by using a relatively conventional design employing leading-edge bluntness and a passive thermal-protection system. The paper addresses the guidance and control required to meet these conditions and thermal modelling is used to determine the cabin temperature rise during re-entry. In comparison with vehicles employing greater aerodynamic sophistication, such as wave-riders, the crossrange is inferior, but in other respects it is shown that the requirements of the re-entry environment can be met.

Keywords: space ambulance; low g re-entry; re-entry trajectory guidance; re-entry thermal modelling; re-entry trajectory modelling

1. Introduction

The rationale for a reusable 'space ambulance' to return ill or injured astronauts from space-station environments has been discussed by Nonweiler (this issue). Physiological constraints on such personnel suggest that the environment in the return vehicle should be as benign as possible from considerations of cabin temperature and g loading during the descent. Also, re-entry on demand is necessary, with the capability of landing at a wide range of landing sites. Thus, significant crossrange capability, which demands a high vehicle lift-to-drag ratio at hypersonic speeds, is required.

These considerations lead to the concept of a low-wing-loading lifting re-entry vehicle to reduce aerodynamic heating, with sufficient cabin volume for the returning astronaut, an attendant, and life and emergency medical support facilities. Particular attention to the thermal design of the vehicle is also necessary, to ensure that not only is the structural integrity preserved, but also that the cabin thermal environment is acceptable during re-entry.

Precision in establishing the acceleration and thermal limits to which the returning ill or injured astronaut is subject is extremely difficult in view of the multiplicity of scenarios that the vehicle is required to meet. However, it is believed that the typical maximum g loading of about $1.5g$ experienced during Space Shuttle re-entry and for the HL-20 Personnel Launch System studied by NASA (see Stone & Piland 1993) would be excessive for many medical emergencies. Little precise quantitative evidence could be found for the g exposure limits for ill or injured personnel, which, in any

case would depend on the nature of the medical condition. However, the upper limit of $1.1g$ suggested for this study is thought to represent a reasonable compromise on the level and duration of the g exposure during return to Earth from a typical space-station orbit. Accordingly, an initial specification for a reusable space-rescue vehicle (RSRV) for use as a space ambulance was established as follows:

capacity	one injured person plus one attendant;
size	to be capable of launch within the Space Shuttle payload bay (60 ft × 15 ft diameter);
maximum g loading	$1.1g$;
mission	return from the International Space Station orbit (51.6°E) and altitude of 220 miles (353 km);
crossrange	up to 3000 km;
landing	horizontal on a conventional runway;
re-entry and landing	fully automatic;
propulsion	for deorbiting manoeuvre and reaction control system during re-entry.

The vehicle design discussed by Nonweiler (this issue) to meet this specification was chosen to incorporate aerodynamic sophistication using 'wave-rider' principles to achieve high lift-to-drag (L/D) ratios. Nonweiler's (this issue) design study shows that the peak g loading requirement can be met and that this does not impose a compromise on the thermal loading of the vehicle, even allowing for the sharp leading edges and the use of a wholly metallic conductive–radiative thermal-protection system.

In this paper an alternative approach to the design of such a vehicle is explored, using a more conventional thermal-protection system employing insulation–radiation and nose leading-edge bluntness, to establish whether the benign re-entry environment specification could be met with this type of vehicle. The conceptual part of this study was carried out by Farquhar, Fishburne and Whittington as an M.Eng. group design project at the University of Southampton (see Farquhar *et al*. 1996). This resulted in a RSRV design somewhat similar in outline concept to the USAF X-20 DynaSoar project that was terminated in 1963.

2. Choice of configuration

The essential purpose of this study was to establish the feasibility of meeting the specification outlined in § 1 by using a relatively conventional configuration. Bearing in mind the requirement for low wing loading, a configuration permitting a simple lightweight structure and associated thermal-protection system was chosen incorporating a blunted-leading-edge flat-bottomed delta planform as the basic shape. Optimum use of the Space Shuttle payload bay, together with aerodynamic considerations, suggested an aspect ratio of 1.0. Nose radius and leading-edge bluntness are determined by the choice of thermal-protection system material. In particular, nose radius has been considered as a design parameter that influences both the maximum surface temperature at the front stagnation point and the vehicle deceleration through its effect on aerodynamic efficiency. Aerodynamic yaw stability and control at both high (during re-entry) and low (during glide and landing) angles of attack

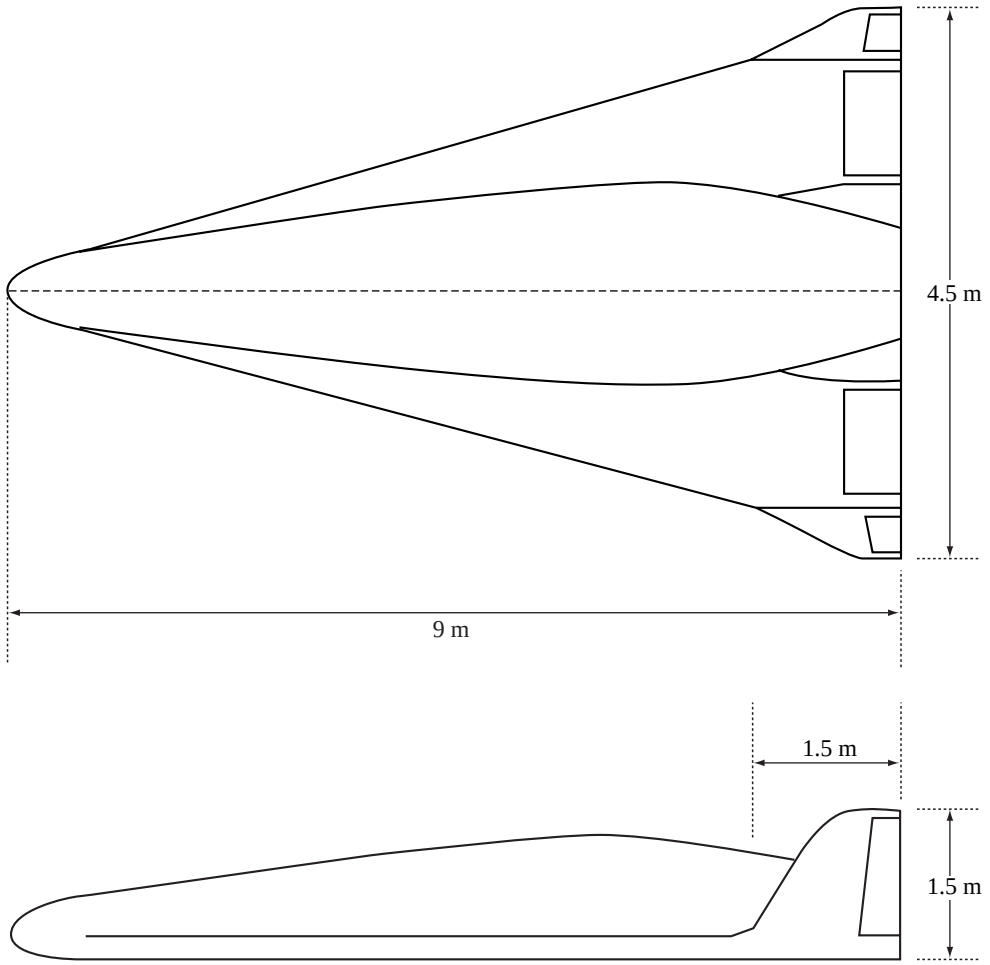

Figure 1. General layout of the reusable space-rescue vehicle.

would be obtained from tip fins. A conventional reaction control system would be used during the initial stages of re-entry.

The two personnel are accommodated in a cabin situated on the upper-wing surface, which is faired into the blunt nose of the vehicle. The approximately semicircular cross-sectional shape is determined by considerations of human factors that require a semiprone position for the medical case, together with sufficient space for the cabin attendant. The increasing influence of base drag at lower Mach numbers requires the base area to be kept low to retain low vehicle deceleration. An adapter would be necessary to enable the transfer of personnel from the space station. A general layout of the RSRV is shown in figure 1.

3. Trajectory and flight-envelope modelling

Evaluation of the design concept was carried out using a re-entry computer model DESCENT coded in FORTRAN. The requirements of this analysis method were to

(i) model all the aerodynamic, gravitational and inertial forces and accelerations acting on the RSRV;

(ii) determine the trajectory of the RSRV due to the action of these forces;

(iii) model the aerodynamic heating of the RSRV at representative surface points (front stagnation point and lower surface midchord in the plane of symmetry);

(iv) model the heating of the cabin; and

(v) allow the implementation of different trajectories and guidance laws.

The re-entry model solves the equations of motion in planar polar coordinates in an inertial reference frame. During re-entry into the atmosphere, the velocity relative to the atmosphere is found by using a rotating spherical Earth model from which the air speed is computed knowing the inertial velocity. In evaluation of the RSRV, the vehicle crossrange from the original orbital plane determines the vehicle's ability to return to as wide a range of landing sites as possible in the event of a medical emergency. Modelling of the crossrange, considering this as an independent parameter, was evaluated by integration of the lateral accelerations caused by out of plane forces due to the vehicle's roll angle. As an aid to the evaluation of the RSRV design, the model was adapted to derive the flight envelope of the vehicle when subject to given constraints of maximum allowable g loading, maximum allowable surface temperature at the nose stagnation point and equilibrium glide. This flight envelope defines the limits of the allowable range of re-entry trajectories and is of central importance in evaluating the feasibility of a particular configuration. It also determines the guidance system specification. The DESCENT software was adapted to produce flight-envelope boundaries for a specific vehicle design subject to the following constraints:

(i) equilibrium glide;

(ii) g loading limits;

(iii) stagnation-point surface temperature limits; and

(iv) lower surface-temperature limits.

The resulting flight envelopes were available in altitude–velocity and drag–velocity space.

The DESCENT computer model simulates the re-entry trajectory by solving the vehicle equations of motion at discrete time-steps. The adaptation of the model to define the flight envelope in terms of altitude and velocity, or equivalently, drag and velocity, was accomplished by converting the code from a time-based, to an altitude-based model (ENVLOP), since the flight boundaries were assumed to be time invariant. To establish the equilibrium glide boundary, an iterative approach was adopted using the vertical acceleration of the vehicle as a measure of the magnitude and direction of the equilibrium velocity. Thus, depending on the magnitude of the vertical acceleration, the vehicle velocity was increased if the vehicle was accelerating downwards and decreased if it was accelerating upwards. This iterative process was necessary since the angle of attack was assumed to be a prescribed function of velocity during re-entry (see § 6 *b* and figure 2).

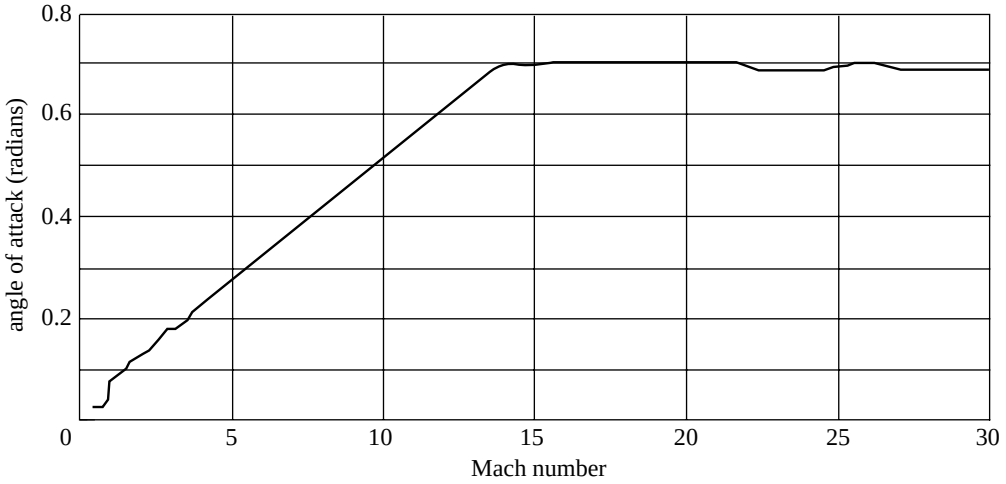

Figure 2. RSRV re-entry angle-of-attack profile.

The loading limit boundary is that imposed by the upper limit of the g loading that is allowable on the occupants of the vehicle ($1.1g$). This loading (in the absence of any propulsive forces) results from the resultant aerodynamic force and the gravitational acceleration acting on the vehicle during re-entry. A similar iterative procedure was adopted as that used for the equilibrium glide boundary, but with the constraint of a maximum g loading of $1.1g$.

Further constraints on the trajectory are imposed by the maximum allowable temperatures of the vehicle structure. In particular, the surface temperature of the insulation at the stagnation point has been considered as a limiting factor. An additional representative point at the midlength of the lower surface was also evaluated, but the stagnation point was found to be the critical parameter. An iterative approach has again been adopted to calculate the required trajectory in the altitude–velocity space that would result in a constant value of the limiting temperature. The surface temperatures of the vehicle are evaluated using the aerodynamic heating and surface thermal models described in § 4. Due to the time-dependent nature of the heat flow into the surface insulation and the supporting structure of the vehicle, the trajectory resulting from the iteration based on constant vehicle surface temperature will not be strictly time independent. However, in practice it was found that a good approximation to the thermal boundary in the altitude–velocity space could be established by using the iterative procedure adopted.

From guidance considerations it is important that the vehicle can execute a re-entry trajectory within the corridor imposed by the boundaries described above. Onboard measurement of vehicle deceleration is the most widely adopted procedure used to effect guidance within the entry corridor This parameter can be sensed with greater accuracy than, for example, altitude and this procedure has been adopted as the basis of the guidance procedure used for the RSRV. Conversion of the flight boundaries from altitude–velocity space to deceleration–velocity space was therefore necessary to derive a reference trajectory along which the vehicle could be guided by its guidance system. This was accomplished by using the drag of the vehicle, which is altitude and velocity dependent, to calculate the deceleration along the flight path

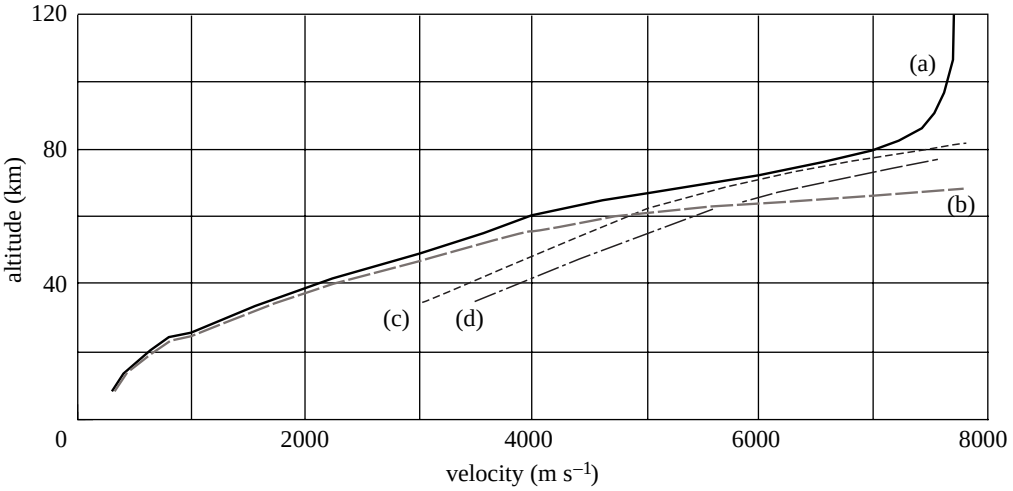

Figure 3. Baseline re-entry flight corridor in altitude–velocity space: (a) equilibrium flight boundary; (b) 1.1g loading boundary; (c) 1800 K stagnation-point surface temperature boundary; (d) 1200 K mid lower surface temperature boundary. Vehicle mass is 7000 kg.

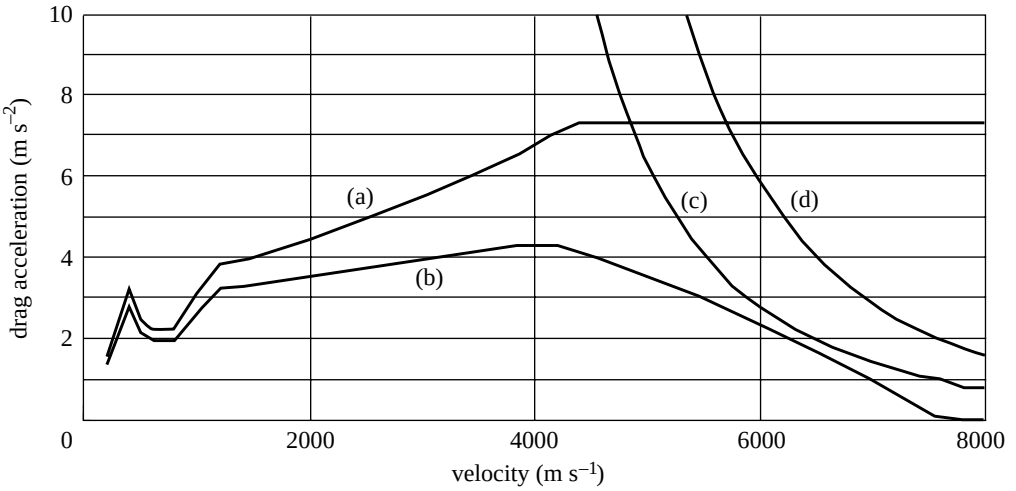

Figure 4. Baseline re-entry flight corridor in drag acceleration–velocity space: (a) equilibrium flight boundary; (b) 1.1g loading boundary; (c) 1800 K stagnation-point surface temperature boundary; (d) 1200 K mid lower surface temperature boundary. Vehicle mass is 7000 kg.

and hence to establish the various flight boundaries in drag acceleration† –velocity space.

Examples of the flight boundaries for the RSRV in altitude–velocity and drag-acceleration–velocity space are shown in figures 3 and 4 for the baseline vehicle having an assumed mass of 7000 kg. These show the boundaries imposed by the constraints of vehicle g loading (1.1g), stagnation-point surface temperature (1800 K), body

† Drag acceleration is defined as the acceleration of the vehicle in the direction of the drag force caused by the drag acting on the vehicle.

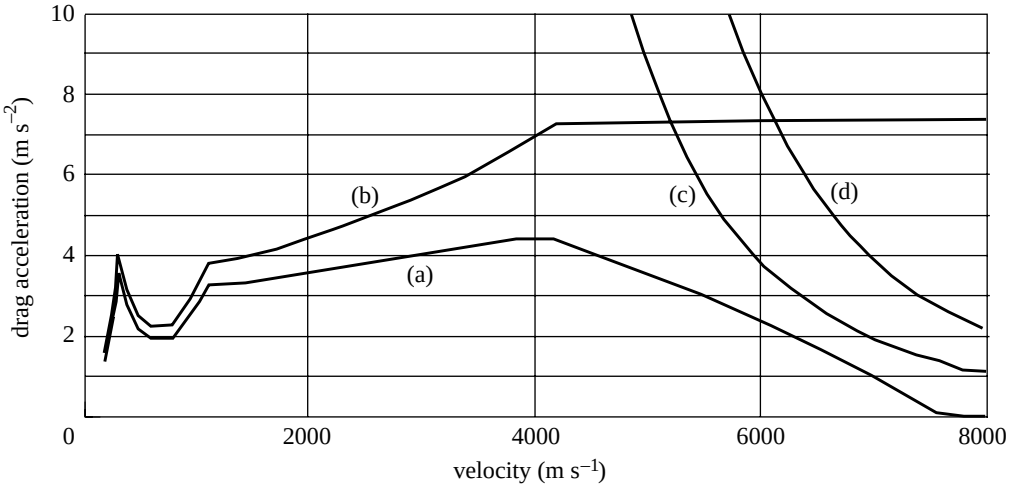

Figure 5. Re-entry flight corridor in drag acceleration–velocity space: (a) equilibrium flight boundary; (b) 1.1g loading boundary; (c) 1800 K stagnation-point surface temperature boundary; (d) 1200 K mid lower surface temperature boundary. Vehicle mass is 5000 kg.

surface temperature (1200 K) and the lower boundary below which the aerodynamic forces are insufficient to maintain equilibrium glide conditions. The irregularities in the deceleration and equilibrium flight boundaries at lower velocities are caused by large changes in the aerodynamic characteristics of the vehicle predicted by the aerodynamic model used for transonic and low supersonic flight conditions (see § 5).

By comparing the flight boundaries for the 5000 kg (figure 5) and 7000 kg (figure 4) vehicle masses, it is noted that the flight corridor for the low-wing-loading vehicle between the stagnation-point surface temperature and the equilibrium flight boundaries is significantly increased over the higher-wing-loading case. Indeed, for the higher-wing-loading case it is only just possible to meet the 1800 K temperature limit with the assumed nose radius of 0.35 m. For a much smaller radius the stagnation surface temperature boundary and the equilibrium flight boundary intersect, resulting in no available flight corridor.

Although no comparable flight envelopes (for which sufficiently precise defining data existed) were available for validation purposes, reasonable qualitative agreement exists between the positions and trends of the boundaries and the Space Shuttle flight envelopes.

4. Vehicle thermal modelling

(*a*) *Vehicle heat balance*

As a contrast to the metallic thermal-protection system (TPS) adopted for the space-rescue vehicle described by Nonweiler (this issue), a relatively conventional insulative–radiative ceramic TPS was chosen for the present study. Detailed unsteady three-dimensional modelling of the heat flow into the vehicle during re-entry was beyond the scope of the present work, so representative points at the front stagnation point and at the midchord ($x = 4.5$ m) of the vehicle lower-surface centreline were chosen for detailed study as the vehicle re-entry proceeded.

The temperatures of representative points on the vehicle surface are evaluated from a locally one-dimensional heat-balance equation accounting for convective heat transfer into the surface, radiative heat transfer away from the surface and non-steady heat conduction into the vehicle insulation and structure. Thus

$$\dot{q}_{\text{conduction}} = \dot{q}_{\text{convection}} - \dot{q}_{\text{radiation}} = \dot{q}_{\text{convection}} - \sigma\varepsilon T_{\text{w}}^4, \tag{4.1}$$

where σ and ε are the Stefan–Boltzmann constant and the surface emissivity, respectively, and T_{w} is the surface temperature.

The convective aerodynamic heating may be written in the approximate form (see Anderson 1989)

$$\dot{q}_{\text{convection}} = \rho_\infty^m V_\infty^n C, \tag{4.2}$$

where the density ρ and the velocity V are based on free-stream conditions and the relationships for the empirical quantities m, n and C are dependent on the location on the vehicle and the boundary-layer state. In SI units these expressions are as follows.

Stagnation point: $m = 3$, $n = 0.5$,

$$C = 1.83 \times 10^{-4} R^{-1/2}(1 - (h_{\text{w}}/h_0)), \tag{4.3}$$

where R is the nose radius in metres and h_{w} and h_0 are the wall and total enthalpies, respectively.

Laminar flat plate: $m = 3.2$, $n = 0.5$,

$$C = 2.53 \times 10^{-5}(\cos\phi)^{1/2}(\sin\phi)x^{-1/2}(1 - (h_{\text{w}}/h_0)). \tag{4.4}$$

Turbulent flat plate: $n = 0.8$,
for $V_\infty < 3962\ \text{m s}^{-1}$, $m = 3.37$,

$$C = 3.89 \times 10^{-4}(\cos\phi)^{1.78}(\sin\phi)^{1.6} x_{\text{T}}^{-0.2} (\tfrac{1}{556} T_{\text{w}})^{-1/2},$$

for $V_\infty > 3962\ \text{m s}^{-1}$, $m = 3.7$,

$$C = 2.2 \times 10^{-5}(\cos\phi)^{2.08}(\sin\phi)^{1.6} x_{\text{T}}^{-0.2}(1 - (1.1 h_{\text{w}}/h_0)),$$

where ϕ is the local body angle with respect to the free-stream, x is the distance along the body surface measured in metres, and x_{T} is the distance measured along the body surface in the turbulent boundary layer.

These relationships are empirically based, but Anderson (1989) has shown that they are representative of the heating rates obtained by more accurate methods and from experiment, and are useful for conceptual analyses.

In this approximate analysis x_{T} is taken as the distance from the origin of the turbulent boundary layer, which is assumed to occur at the transition point. In reality the effective origin of the turbulent boundary layer will be ahead of this point, and for exact analysis account should be taken of the evolution of the whole transition region. For the present study x_{T} has been obtained by using a value of the transition Reynolds number ($Re_{\text{tr}} = \rho_1 V_1 x_{\text{T}}/\mu_1$) of 1.0×10^6, and from a knowledge of the local density ρ_1, velocity V_1 and viscosity μ_1 based on local surface conditions, which are functions of the free-stream conditions and the angle of the vehicle lower surface to the free-stream. These are calculated using oblique shock theory (with $\gamma = 1.4$) based on the angle of attack of the flat lower surface.

Table 1.

location	stagnation point	midlength of body ($x = 4.5$ m)
TPS type	carbon–carbon	HRSI
thickness (m)	0.2	0.045
density (kg m^{-3})	1656	144
heat capacity (J kg^{-1} K^{-1})	775	1047
thermal conductivity (W m^{-1} K^{-1})	1.34	0.075
emissivity	0.9	0.85

Table 2.

mass of cabin and contents	430 kg
average heat capacity of contents	4190 J kg^{-1} K^{-1}
cabin length	4.5 m
cabin diameter	1.5 m
thermal conductivity of insulation	0.038 W m^{-1} K^{-1}
thickness of insulation	0.025 m

(*b*) *Thermal-protection system heat conduction*

The variation of the vehicle surface temperature throughout the re-entry trajectory was calculated using the thermal balance model given by equation (4.1). The heat conduction into the vehicle was modelled using a non-steady one-dimensional heat flow into the TPS. Lateral heat conduction was not taken into account with the result that the stagnation-point surface temperature was overestimated. The vehicle TPS was modelled as a layer of uniform insulation supported on an aluminium alloy structure. For the stagnation region, carbon–carbon insulation was used as for the Space Shuttle and the proposed HL20 vehicle. For the representative midchord lower-surface position, high-temperature reusable surface insulation (HRSI) in the form of ceramic tiles was assumed. The thermal properties of the TPS used in the calculations are shown in table 1.

The estimation of the temperature of the front stagnation point also requires a knowledge of the effective radius of the nose of the vehicle. The nose shape proposed was a portion of a sphere, suitably blended into the flat lower-surface contour, the blunted leading edge of the slender delta planform, and the upper-surface contour that incorporates the cabin. For the re-entry phase at which the highest stagnation-point temperatures occur it is necessary for the angle of attack to be high (40°). At these conditions the blending into the lower surface and the shift of the front stagnation point away from the vehicle apex would result in an increased effective radius at the front stagnation point. This factor, coupled with the omission of lateral heat conduction, will result in a conservative design for the nose region TPS.

(*c*) *Cabin temperature*

Heating of the vehicle's cabin and its contents (injured or sick person, attendant, life-support systems, medical equipment, etc.) was modelled by assuming a

cylindrical pressure vessel surrounded by an annular layer of low-temperature insulation, the outer-surface temperature of which was taken to be the temperature of the vehicle aluminium skin structure obtained using the one-dimensional non-steady heat-transfer model of the vehicle TPS. The temperature rise of the cabin contents was calculated using the lower-surface midlength reference value as an average acting over the whole surface of the cabin. This should lead to an overestimate of the cabin temperature since the midlength of the cabin aft of the midchord position and the upper part of the vehicle structure will be substantially cooler than that of the lower structure. The physical properties of the cabin contents and insulation used in the calculation are given in table 2.

5. Aerodynamic modelling

(*a*) *General*

Analysis of the critical re-entry trajectory of the RSRV required the development of an aerodynamic model from which the aerodynamic characteristics over the flight regime $0 < M < 30$ could be estimated. The scope of this study did not justify the development of computational fluid dynamic methods over such a wide range of Mach number and angle of attack ($0° < \alpha < 40°$) and consequently an integrated analytical model was adopted using semiempirical methods appropriate to the various flight regimes from hypersonic to subsonic.

The generic shape chosen for these studies was a flat-bottomed delta planform (for high-supersonic/hypersonic L/D), with a hemispherical nose and blunted leading edges (for acceptable maximum surface temperatures), twin tip fins (for lateral stability), sufficient body volume to house the two occupants with high length-to-width ratio (to minimize sub/supersonic drag) and small base area (to minimize sub/supersonic base drag). The design specification required high L/D to enable the g loading and crossrange requirements to be met. This was compromised by the requirement for the stagnation-point surface temperature not to exceed 1800 K, which resulted in blunting of the vehicle apex and a reduction in L/D.

(*b*) *Hypersonic aerodynamics*

The hypersonic characteristics were based on modified Newtonian aerodynamics, with the pressure coefficient factor and its variation with Mach number and angle of attack obtained from empirical data reported by Hankey (1988). Semiempirical data for laminar and turbulent skin friction were obtained from Hankey (1988), which are valid for flat surfaces over a range of angles of attack at hypersonic Mach numbers. Hankey (1988) has applied these results to a generic re-entry vehicle, the lower surface and leading-edge shape of which closely resemble that chosen for the RSRV. Hence it was possible to use the expressions derived by Hankey for the normal and tangential force coefficients due to the various components of the vehicle, for the specific RSRV geometry. These expressions were used for Mach numbers above 4.0.

(*c*) *Supersonic aerodynamics*

For Mach numbers between 4 and 1, two methods were used to obtain approximate aerodynamic characteristics dependent on whether the leading edges were

supersonic or subsonic. For the subsonic leading-edge case, McCormick (1995) provides expressions for the induced drag taking into account leading-edge suction. For the supersonic leading-edge case, semiempirical methods quoted by Raymer (1992) have been used to estimate the contributions of skin friction, base and wave drag. For the latter, a value of 1.4 for the ratio of the actual wave drag to that of the ideal Sears–Haack body was adopted for the RSRV.

(*d*) *Subsonic aerodynamics*

In the conceptual evaluation of the overall re-entry trajectory performance of the RSRV the subsonic aerodynamic performance is relatively unimportant and estimates of C_{L} and C_{D} of sufficient accuracy were obtained by using the characteristics of a flat delta wing modified for compressibility effects on C_{L} and induced drag coefficient C_{Di}. Raymer's (1992) semiempirical methods were used for estimating the contributions of skin friction and base drag for a delta wing/body combination. Subsonic aerodynamics are, of course, very important for terminal guidance and control and for obtaining a bump-free landing.

(*e*) *Integrated aerodynamic model*

The foregoing methods were integrated into an overall aerodynamic model that was used in the computational analysis of the complete re-entry trajectory. This enabled the important interactive effects between the permitted maximum surface temperature resulting from the choice of nose bluntness and the g loading on the vehicle arising from its drag to be evaluated. The aerodynamic model was also used in determining the shape of the blended cabin and its base area that could be tolerated from an aerodynamic viewpoint, yet would be consistent with the logistical considerations of access of personnel to the cabin from the space station. Parametric investigations of the effect of the maximum cabin width and base area over the operating range of supersonic and hypersonic Mach numbers enabled design compromises, effective over this flight regime, to be reached.

6. Guidance and trajectory control

(*a*) *Guidance*

A guidance system must be chosen that enables a trajectory to be flown within the entry corridor defined by the RSRV thermal, g loading and equilibrium flight boundaries (see § 3). The guidance system must guide the vehicle along an entry trajectory, not only consistent with the above constraints, but also compatible with further requirements imposed by minimum re-entry duration (if medical circumstances are critical) and landing-site targeting (requiring control over downrange and crossrange).

The basic concept adopted is similar to that used by the Space Shuttle and described by Harpold & Graves (1979) and which was also proposed by Cledassou (1992) for the European Hermes vehicle and by Lu & Hanson (1998) for the X-33 vehicle. For this system the vehicle is constrained to fly down a precalculated optimum trajectory for the current vehicle and atmospheric conditions through the use of guidance feedback loops on the roll and pitch angles. Although differing in

detail, all these systems are based on the vehicle tracking a nominal drag acceleration profile.

The re-entry is initiated by a deorbit burn, the magnitude of which is computed to result in an angle of entry at the atmospheric interface within the limits required to prevent skip and to prevent surface overheating, and to keep the g loading on the occupants within the $1.1g$ limit. Engine underburn at deorbit can be compensated by the guidance system controlling the roll angle at the atmospheric interface from the normally zero roll angle at this position.

(*b*) *Atmospheric deceleration guidance*

Starting at the atmospheric interface, the deceleration guidance system controls the vehicle through the most stringent constraints (temperature and deceleration) in the high-speed portion of the trajectory prior to the landing guidance phase. Considerations of surface temperature, minimum duration of the trajectory (high drag) and stability of the vehicle, require that a high angle of attack is flown at the highest Mach numbers, reducing to a low value at lower supersonic Mach numbers. The angle-of-attack profile is, therefore, prescheduled (as described by Messerschmidt & Schöttle (1991)), apart from small control inputs, as shown in figure 2. The implication is that, since the angle of attack is so tightly limited, the majority of the trajectory is controlled through the use of roll. Using this angle-of-attack profile and imposing the temperature, g loading and equilibrium flight constraints enables a re-entry flight trajectory to be deduced in altitude–velocity space. As described in § 3, drag acceleration is chosen as the most accurately measurable internal parameter to be used as the trajectory control parameter. Furthermore, its variation is unique for each combination of altitude and velocity, enabling straightforward transformation from altitude–velocity to drag acceleration–velocity space. An example of the entry corridor transformed into drag acceleration–velocity space is shown in figure 3. The space within the temperature, g loading and equilibrium flight boundaries defines the regime of allowable entry trajectories. However, the additional constraint of minimum entry duration requires that the trajectory flown should closely follow the temperature and g loading boundaries. This defines a reference profile, along which the vehicle should be guided for minimum duration. Other reference profiles, within the flight corridor, may be chosen if increased downrange and crossrange trajectories, but with increased duration, are required. Such trajectories would generally result in increased cabin temperatures due to the prolonged high-temperature flight regime.

(*c*) *Trajectory control logic*

As mentioned above the angle-of-attack profile is assumed to be predetermined and variation of the roll angle is used as the principal parameter to control the vehicle along the reference trajectory in drag acceleration–velocity space. A relationship between drag acceleration a_{d} and roll angle ϕ may be found from the following analysis, which assumes a small flight-path angle:

$$D = ma_{\mathrm{d}}, \qquad L_{\mathrm{v}} - W' = 0,$$

where D is the drag, L_{v} is the vertical component of the lift and W' is the effective weight, i.e. the vehicle weight minus the vehicle mass m times the centripetal

acceleration. Hence,

$$a_{\mathrm{d}} = (L_{\mathrm{v}}/D)^{-1}(W'/m).$$

The drag acceleration may, therefore, be modulated by changing the vertical component of the lift, that is by varying the roll angle ϕ according to the following expression:

$$\phi = \cos^{-1}\left(\frac{L_{\mathrm{v}}/D}{L/D}\right),$$

where L is the total lift acting on the vehicle.

The total lift-to-drag ratio L/D can be found from internally measured accelerations and the roll angle ϕ can be adjusted to give the required value of a_{d}. Any deviations from the reference profile caused by atmospheric or other factors are compensated by a feedback error-control term based on the sensed deviation of the drag acceleration from that required by the reference profile. A further term that limits the rate at which flight-path angle can change is introduced to compensate for short-term deviations from the reference profile. The final form of the vertical lift-to-drag ratio command equation is

$$(L/D)_{\mathrm{command}} = (L/D)_{\mathrm{ref}} + k_{\mathrm{d}}(a_{\mathrm{d}} - a_{\mathrm{d\,ref}}) + k_{\dot{\gamma}}(\dot{\gamma} - \dot{\gamma}_{\mathrm{ref}}),$$

where k_{d} and $k_{\dot{\gamma}}$ are the system gains, a_{d} and $a_{\mathrm{d\,ref}}$ are the sensed and reference drag accelerations, respectively, and $\dot{\gamma}$ and $\dot{\gamma}_{\mathrm{ref}}$ are the sensed and reference rates of change of the flight-path angle.

Although the angle-of-attack profile is prescheduled, a low-gain feedback loop based on the drag acceleration error is introduced to help counter unexpected atmospheric gradients, together with the effects of roll reversal necessary to control cross-range. The angle-of-attack command equation is

$$\alpha_{\mathrm{command}} = \alpha_{\mathrm{ref}} + k_{\alpha}(a_{\mathrm{d}} - a_{\mathrm{d\,ref}}),$$

where k_{α} is the angle-of-attack feedback gain.

7. Results and discussion

(*a*) *Baseline data*

In § 3 the re-entry corridor and hence a reference flight profile was defined to meet the constraints of temperature, g loading and equilibrium flight. In § 6 the guidance and control strategy, employing variation in roll angle, required to enable the vehicle to fly the reference flight profile, was described. Using this approach and the DESCENT software described in § 3, the ability of the chosen design to meet the design specification (see § 1) has been evaluated. The principal parameters that have been used for the baseline design are summarized in table 3.

Firstly, it is noted that for this conceptual study little structural design work has been done and consequently accurate mass estimation has not been possible. However, from comparison with existing designs and from a knowledge of the probable masses of the payload, on-board guidance and control systems, life-support systems, thrusters for deorbit and control, undercarriage, etc., it seems likely that the total

Table 3.

mass	7000 kg
length	9 m
span	4.5 m
nose radius	0.35 m
wing loading	3457 N m^{-2}
maximum surface stagnation temperature	1800 K
maximum body reference temperature	1200 K
initial orbit height	220 miles (353 km)
initial orbit inclination	51.6° E

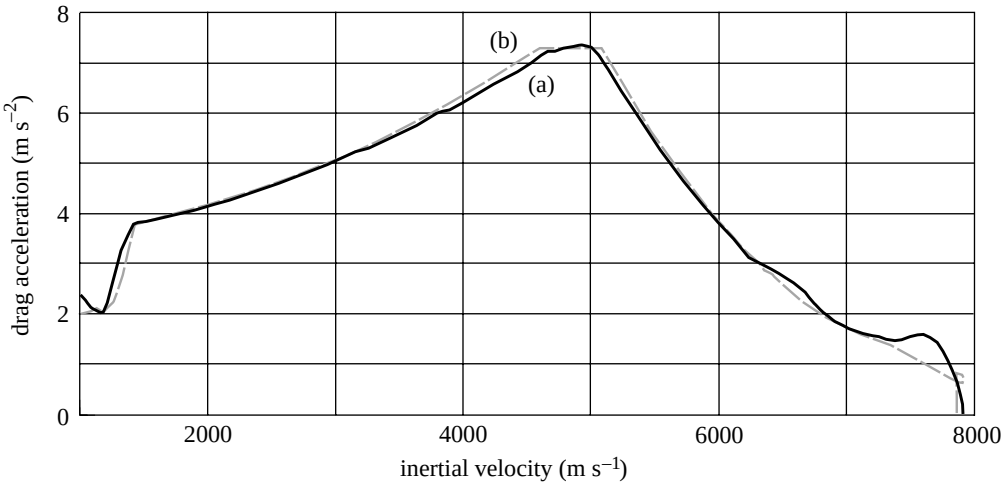

Figure 6. Trajectory control: comparison of (a) the actual re-entry profile with (b) the reference profile in drag acceleration–velocity space.

mass should not exceed the baseline value of 7000 kg. In view of the uncertainty in the mass estimation, the effects of lower masses of 5000 kg and 3000 kg have also been explored.

The simulated re-entry flight profile in the drag acceleration–velocity space is shown in figure 6. This demonstrates the ability of the control logic described in § 6 to enable the baseline vehicle to follow the computed reference profile during a simulated re-entry trajectory. The only portion of the trajectory where there is departure from the reference profile is during the early stages of re-entry where the aerodynamic forces available from variation in the roll angle and from angle-of-attack modulation were insufficient to effect complete control. The baseline re-entry trajectory is also shown as variation of altitude and velocity with time from deorbit in figure 7.

(*b*) *Aerodynamic performance*

A measure of the aerodynamic performance of the RSRV during re-entry is the effectiveness of the vehicle in simultaneously maintaining high values of C_{L} and L/D. Pike (first paper, this issue) has derived the following parameters to compare

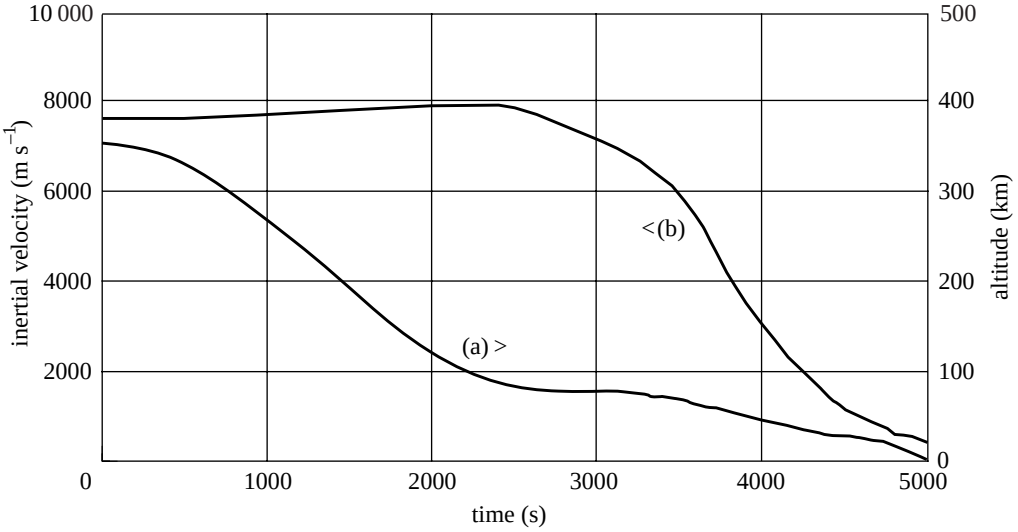

Figure 7. Variation of altitude and velocity with time from deorbit for baseline RSRV: (a) altitude; (b) inertial velocity.

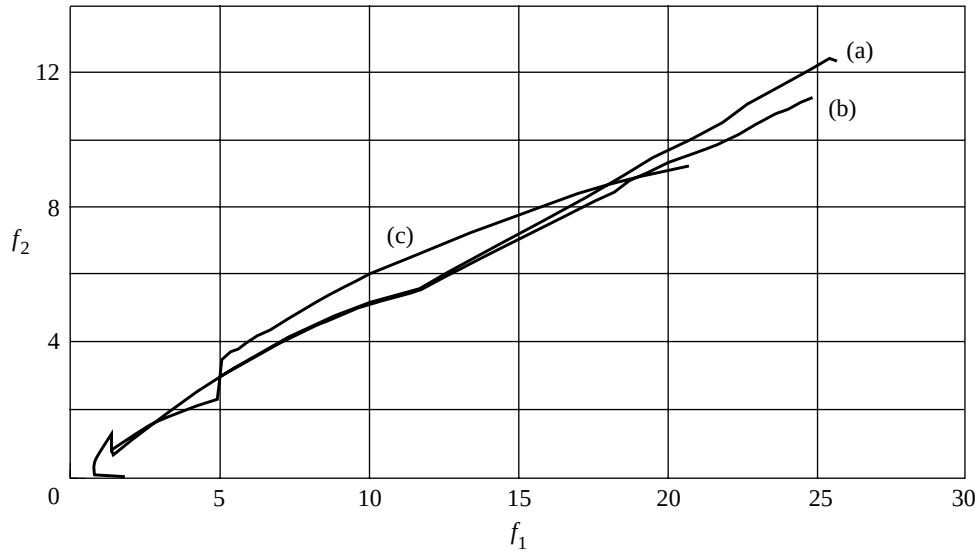

Figure 8. Aerodynamic performance of the RSRV during the re-entry trajectory using parameters due to Pike (first paper, this issue) $f_1 = C_{\mathrm{L}}^{1/2} M_\infty^2 / \sqrt{(M_\infty^2 - 1)}$ and $f_2 = \frac{1}{2} C_{\mathrm{L}} (L/D)(M_\infty^2 - 1)^{1/2}$: (a) RSRV–pressure forces only; (b) RSRV with skin friction included; (c) Nonweiler's (this issue) waverider with skin friction included.

the effectiveness of different vehicles in meeting this criterion:

$$\tfrac{1}{2} C_{\mathrm{L}} (L/D)(M_\infty^2 - 1)^{1/2}, \qquad C_{\mathrm{L}}^{1/2} M_\infty^2 / \sqrt{(M_\infty^2 - 1)}.$$

The variation of these parameters throughout the re-entry trajectory is shown in figure 8. Two curves are shown for the RSRV for the cases of (a) pressure forces only and (b) with skin friction included. Comparison of these curves shows the relatively

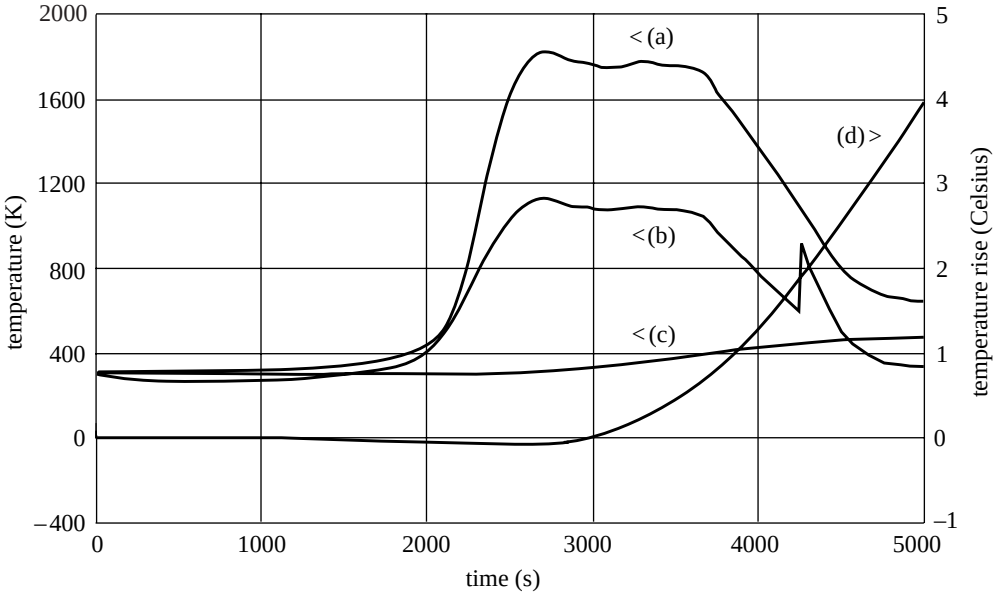

Figure 9. Temperature variation with time from deorbit for baseline RSRV: (a) stagnation-point surface; (b) lower midchord ($x = 4.5$ m) surface; (c) lower midchord ($x = 4.5$ m) structure; (d) cabin interior temperature rise.

greater effect of skin friction at the low Reynolds numbers prevailing during the high-altitude high-Mach-number phase of re-entry. Comparison is also made with the aerodynamic performance of the SLEEC space-ambulance concept described by Nonweiler (this issue). Firstly, it is noted that the RSRV vehicle commences its re-entry at higher values of C_{L}, since the initial entry is accomplished at a higher angle of attack. However, for the majority of the trajectory, the SLEEC vehicle has higher values of the product $C_{\mathrm{L}}(L/D)$ as a consequence of its more aerodynamically efficient sharp-leading-edge waverider shape, rather than the blunted nose and leading-edge configuration adopted for the RSRV. The predominant effect of the superior aerodynamic performance of the SLEEC vehicle is the increased maximum crossrange, in excess of 3000 km, compared with some 2150 km for the baseline RSRV when similar constraints of apex temperature and g loading are applied. This demonstrates that although there are significant advantages in adopting existing technology for thermal protection in the RSRV, these result in some compromise in the number of landing sites that could be reached after deorbit and re-entry.

(*c*) *Temperature*

The variation of the surface temperature at the front stagnation point throughout the flight trajectory is shown in figure 9. The guidance and control strategy, using variation of roll angle, outlined in § 6, results in a temperature controlled to within *ca.* 2% of the limit of 1800 K. The duration of the exposure to the limiting temperature is *ca.* 1000 s, during which period the lower-surface reference temperature at $x = 4.5$ m is comfortably less than the limiting value of 1200 K. After 3200 s from deorbit, the temperatures fall as the g limit becomes the overriding factor. However,

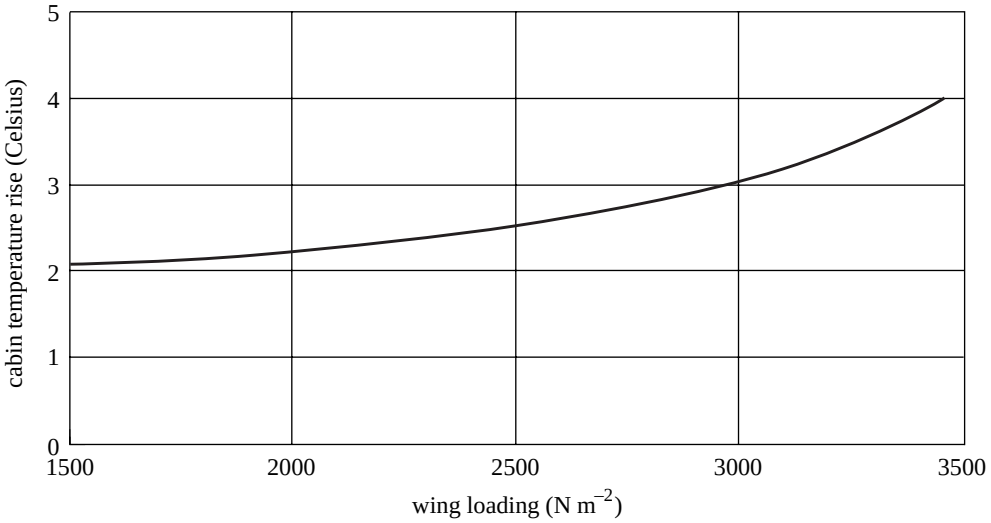

Figure 10. Effect of wing loading on cabin temperature rise.

at 4200 s an increase in the lower-surface temperature occurs, although to a value below the limiting value of 1200 K, as a result of transition-to-turbulent boundary-layer behaviour on the lower surface.

The variation in the temperature of the vehicle structure beneath the insulation at the lower-surface midchord point is also shown in figure 9. This demonstrates the considerable lag in the build-up of the structure temperature to a maximum of 470 K, which is reached at the end of the trajectory.

Figure 9 also shows the change in the cabin temperature during re-entry. For the period up to 3000 s from deorbit a small decrease in temperature occurs due to the dominant effect of the radiation heat-loss term and lack of a solar-radiation heat-input term in the heat-balance equation before the convective heating assumes importance as the atmospheric interface is passed. The major feature of the evolution of the cabin temperature is the considerable lag in its response to the aerodynamic heating due to the extensive insulation. Indeed, it would be expected that the cabin temperature would continue to rise after landing due to thermal soak of the vehicle. For the system modelled, the increase in temperature of the cabin contents is *ca.* 4 °C, which is reached at the point of landing, demonstrating that it is possible to maintain a tolerable cabin thermal environment using only a passive thermal control system as described in § 4. Reduction of vehicle wing loading reduces the cabin temperature rise as shown in figure 10. This results from the shorter period of exposure to the highest temperatures and from the relatively higher trajectory flown during the hypersonic glide.

(*d*) *g loading*

Figure 11 shows the variation of the g loading experienced by the vehicle and its occupants during the re-entry from the time of deorbit. The g increases during the temperature-limiting phase of re-entry and reaches a value of *ca.* 1.1 g at 3650 s, which roughly coincides with the end of the temperature-limiting phase. From this point onwards the guidance and control system is effective in maintaining the g

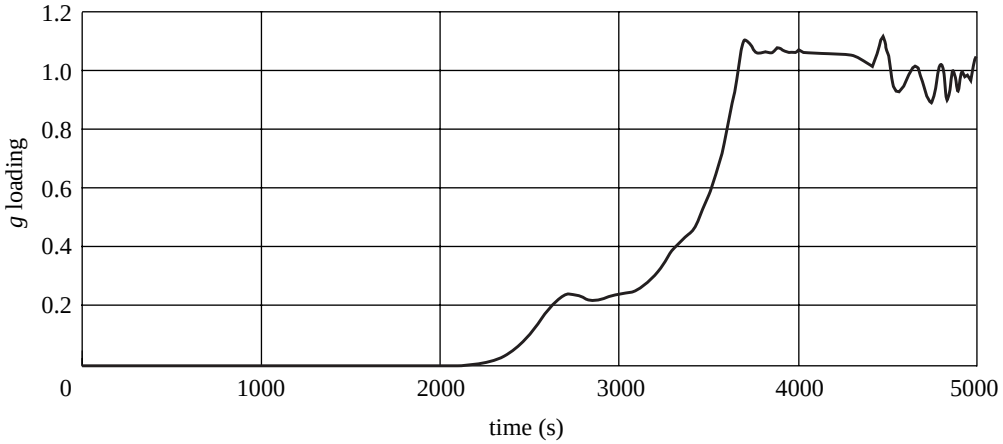

Figure 11. Variation of g loading with time from deorbit.

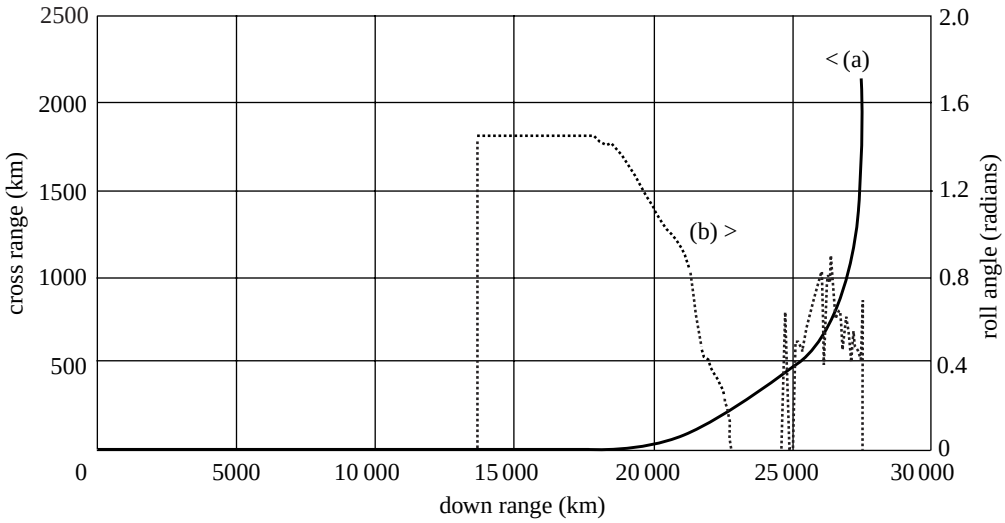

Figure 12. (a) cross-track of RSRV and (b) roll angle during re-entry.

loading below the specified value ($1.1g$), apart from a short duration excess of *ca.* 3% at $t = 4450$ s due to rapid changes in aerodynamic characteristics resulting from a locally unrealistic aerodynamic model as a particular boundary between flight regimes is transgressed. Similar variations in g loading continue to occur after this and are due to related causes as various regimes used in the aerodynamic model are passed. Similar evaluations (not shown), demonstrate that it is equally possible to keep within the g loading limit of $1.1g$ for assumed vehicle masses of 5000 kg and 3000 kg.

(*e*) *Ground-track and crossrange*

During the re-entry trajectory the required reference flight profile is flown using roll angle as the controlling parameter. The maximum crossrange is achieved when

all of the roll control inputs are in the same direction. This maximum crossrange is shown in figure 12 as a function of distance downrange from the point of deorbit. For the baseline design, a maximum crossrange of 2150 km is achieved. Also shown in figure 12 is the variation of roll angle of the RSRV during the descent. Should the particular landing site require less crossrange, roll reversal would be employed to modulate the crossrange while still maintaining the same reference flight profile and downrange.

8. Concluding remarks

This conceptual design study has proposed a relatively conventional blunted flat-bottomed delta configuration as a reusable space-rescue vehicle capable of an emergency return from space-station orbit with an injured or sick astronaut accompanied by an attendant. Simulated re-entry studies have demonstrated that the vehicle can meet a design specification within the $1.1g$ maximum during re-entry and with a cabin temperature rise of no more than 4 °C. The vehicle employs existing technology for its thermal-protection system and has a limiting stagnation-point surface temperature of 1800 K. Comparisons with a waverider-based space-ambulance concept proposed by Nonweiler (this issue) have shown that although the RSRV has inferior aerodynamic performance, it is capable of meeting similar benign re-entry requirements, but with a reduced crossrange of 2150 km compared with in excess of 3000 km for the waverider vehicle.

The author acknowledges the significant contributions of his M.Eng. Group Design Project students, Jason Farquhar, Andrew Fishburne and Matthew Whittington to the work described in this paper. He also gratefully acknowledges many helpful discussions with Dr L. H. Townend of APECS Ltd.

References

Anderson Jr, J. D. 1989 *Hypersonic and high-temperature gas dynamics*. New York: McGraw-Hill.

Cledassou, R. 1992 Hermes rescue trajectories. *Adv. Astronaut. Sci.* **67**, 1041–1061.

Farquhar, J., Fishburne, A. & Whittington, M. 1996 The conceptual design of a reusable space rescue vehicle. M.Eng. Group Design Project, University of Southampton, UK.

Hankey, L. W. 1988 *Re-entry aerodynamics*. AIAA Education Series. Washington, DC: American Institute of Aeronautics and Astronautics, Inc.

Harpold, J. C. & Graves, C. A. 1979 Shuttle entry guidance. *J. Astronaut. Sci.* **37**, 239–268.

Lu, P. & Hanson, J. M. 1998 Entry guidance for the X-33 vehicle. *J. Spacecraft Rockets* **35**, 342–349.

McCormick, B. W. 1995 *Aerodynamics, aeronautics and flight mechanics*, 2nd edn. New York: Wiley.

Messerschmidt, E. & Schöttle, U. M. 1991 Atmospheric re-entry of capsules and winged Vehicles. Re-entry Technology, Space Course, Aachen.

Raymer, D. P. 1992 *Aircraft design: a conceptual approach*. AIAA Education Series. Washington, DC: American Institute of Aeronautics and Astronautics, Inc.

Stone, H. W. & Piland, W. M. 1993 21st century space transportation system design approach: HL-20 personnel launch system. *J. Spacecraft Rockets* **30**, 521–528.